Using AFM Force−Distance Curves To Study the Glass-to-Rubber Transition of Amorphous Polymers and Their Elastic−Plastic Properties as a Function of Temperature

B. Cappella,* S. K. Kaliappan, and H. Sturm

Federal Institute for Material Testing and Research, Berlin, Germany

Received August 23, 2004

ABSTRACT: Force−displacement curves have been obtained with a commercial atomic force microscope (AFM) at different temperatures and probe rates on a thick film of poly(*n*-butyl methacrylate) (PnBMA). The analysis of the force−displacement curves has been focused on the contact portion of the curves, giving information about the stiffness of the sample and its Young's modulus. A novel model of sample deformations that extends the basic equations of the elastic continuum contact theories to the plastic deformations is presented. This model gives several insights into the processes of deformation of soft samples and permits to calculate not only the parameters of the Williams−Landel−Ferry equation but also the Young's modulus and the yielding force of the polymer as a function of temperature and/or probe rate. These quantities have been measured in a wide range of temperatures (70 K) and probe rates (6 decades) for the first time with the AFM, and the results are in very good agreement with measurements performed with customary techniques, such as broadband spectroscopy and dynamic mechanical analysis.

Introduction

One of the most important parameters characterizing a polymer is the glass transition temperature T_g. Several physical quantities of the polymer assume considerably different values below and above T_g. The Young's modulus E, for instance, may decrease 3 orders of magnitude around T_g.

In the past 5 years there has been a great deal of work aimed to the determination of T_g through atomic force microscopy (AFM) measurements[1] and in particular through the acquisition of force−displacement curves.[2−4]

In a first publication of Marti et al.,[2] the authors have observed that the adhesion of polystyrene dramatically increases above a certain temperature depending on the molecular weight of the polymer.

A more exhaustive experiment, also dealing with the adhesion between tip and sample, is that of Tsui et al.[3] The authors have acquired force−displacement curves at different frequencies and temperatures and have been able to draw a master curve of the adhesion.

Finally, Bliznyuk et al.[4] have calculated several quantities from force−displacement curves acquired at different frequencies and temperatures and have shown that all these quantities change abruptly at $T = T_g$. Unfortunately, except for the pull-out force, all the quantities measured by these authors have no clear relationship with some physical properties of the polymer sample, so that the experiment is rather a method to determine T_g instead of giving some insights into the physical processes occurring at $T = T_g$ and into the dependence of physical quantities, e.g., stiffness or hardness, on temperature and frequency.

Also, the measurement of the Young's modulus E of various samples has made great strides in the few past decades.[5]

The theoretical work of Maugis[6] has combined all previous elastic continuum contact theories[7−9] in a complete and general description, showing the limits, but also the possibilities, of AFM measurements of the elastic properties of samples. Several publications have shown that the quantitative determination of the Young's modulus and the comparison between AFM data and those supplied by other experimental techniques is possible also for polymers.[10−14]

The situation is completely different in the case of plastic deformations. In this field there are very few significant theoretical and experimental results.[14] Yet, the study of plastic deformations and of the yield strength has a great importance for polymers.

All the quantities mentioned above can be measured also with well-established techniques, e.g., dynamic mechanical analysis (DMA). The peculiarity of AFM measurements is the capability to perform local measurements with a lateral resolution on the nanometer scale. This gives the opportunity to observe stiffness or T_g differences in finely structured polymer samples, e.g., copolymers with domains larger than ca. 100×100 nm^2.

In this paper we present measurements of force−displacement curves on poly(*n*-butyl methacrylate) (PnBMA) at different temperatures and frequencies. A novel analysis of the data, including a model of the plastic deformations, permits not only to determine the glass transition temperature of the polymer but also, for the first time, to characterize the whole dependence of the Young's modulus and of the yield strength in the vicinity of T_g.

Experimental Section

Samples. Poly(*n*-butyl methacrylate) (PnBMA) was purchased from Scientific Polymer Products, Inc., Ontario, NY, and was used without further purification. The molecular weight, the polydispersity index, and the glass transition temperature given by the supplier are $M_w = 319$ kDa, $M_w/M_n \leq 2.58$, and $T_g = 22$ °C.

Films of PnBMA were prepared by casting saturated solutions of the polymer in toluene. The large thickness of the samples (more than 1 mm) permits to perform large indentations without undesirable artifacts due to the large stiffness of the substrate.[15] To neglect the effect of substrate, the indentation depth should not exceed 10% of the thickness of the film.[16] Prior to the initial study, samples were dried at room temperature for 2 weeks.

10.1021/ma040135f CCC: $30.25
Published on Web 02/05/2005

Techniques. Atomic force microscopy (AFM) measurements were performed with a MFP-3D (Asylum Research, Santa Barbara, CA). A rather stiff cantilever has been used for the acquisition of force−distance curves. If the cantilever's spring constant is smaller than the elastic modulus of the sample, force−displacement curves will probe primarily the cantilever stiffness.[5] Furthermore, one of the aims of the experiment is to provoke large plastic deformations. On the other hand, if the cantilever's spring constant is too high, the force resolution would be very bad. Hence, Pointprobe NCL cantilevers (Nanosensors, Wetzlar-Blankenfeld, Germany) with elastic constant $k_c = 45$ N/m and Si tips have been employed for all measurements.

Force−displacement curves have been acquired at different temperatures (from 30 to 51 °C over 33, 36.5, 40.5, 43.5, and 46 °C) by heating the basis of the polymer sample through a miniature metal plate controlled by a 340 temperature controller (Lake Shore Cryotronics, Westerville, OH). The temperature of the polymer surface has been measured directly with a PT100 fixed on the sample surface. For each temperature the sample has been heated overnight, so that it could reach an equilibrium temperature, which stayed constant for several days (±0.3 °C measured on the surface).

The repeatability of the force−displacement curves measurements has been checked at the end of the temperature cycle.

For each temperature force−displacement curves have been acquired at different frequencies (usually 30, 10, 1, 0.5, 0.1, and 0.03 Hz) with high sampling density. Since the minimum step of the vertical piezo displacements is 1 pm and the piezoactuator acts like a capacitor, the piezoactuator displacement has been assumed to be continuous, and the probe rate is the frequency of the piezoactuator displacement, i.e., the frequency of the force−displacement curve.

For each temperature and frequency a variable number of force−displacement curves (from 100 up to 400) has been acquired. The total number of force−displacement curves taken into account for the analysis is ca. 11 500. Each group of 100 force−displacement curves has been acquired on different areas of the sample (usually 30 × 30 μm^2) in force−volume acquisition mode; i.e., all curves start from a fixed absolute height, an approach−withdrawal cycle is performed, then a lateral displacement, again an approach−withdrawal cycle, and so on. Small variations of the sample topography and variations of the starting height permit the sampling of a large indentation range, from some 10 nm up to 500 nm for curves at high temperatures and/or low frequencies.

Dynamic mechanical analysis (DMA) measurements have been performed with a Netzsch DMA 242 C (Germany). The temperature range was −60 to 100 °C, with a heating rate of 3 K/min. The frequency range was 0.1−100 Hz. The complex Young's modulus was calculated from the equation $E^* = (l/A)(F^*/a^*)$, where a is the amplitude of oscillations (10 μm), A is the surface area of the sample, l is the length (9 mm), and the force F is controlled in order to hold the amplitude constant.

In broadband spectroscopy measurements the complex dielectric function $\epsilon^*(\nu) = \epsilon'(\nu) - i\epsilon''(\nu)$ ($i = \sqrt{-1}$, ν is the frequency, ϵ' is the real part, and ϵ'' is the imaginary part) was measured in the frequency range from 10^{-2} to 10^7 Hz by a high-resolution dielectric spectrometer (Alpha-Analyzer, Novocontrol).[17] The temperature of the sample was controlled by a nitrogen gas jet cryostat with a temperature stability better than 0.1 K (Quadro-System, Novocontrol). The investigations cover a temperature interval from −20 to 120 °C.

To estimate the relaxation rate at maximal loss ν_m connected to the mean relaxation time τ by $\nu_m = 1/(2\pi\tau)$ for each process, the model function of Havriliak−Negami (HN) $\epsilon^*_{HN}(\nu) = \epsilon_\infty + \Delta\epsilon/[(1 + (i\nu/\nu_0)^n)^m]$ was fitted to the data.[18] ν_0 is a characteristic frequency close to ν_m, ϵ_∞ is ϵ' for $\nu \gg \nu_0$, and $\Delta\epsilon$ is the relaxation strength. The fractional shape parameters n and m ($0 < n$, $nm \leq 1$) describe the symmetric and asymmetric broadening of the relaxation spectra, respectively, compared to a Debye relaxation function.[17] If two relaxation processes are observed in the measuring frequency window, two HN functions are fitted simultaneously to the data. The conductivity contribution to the dielectric loss was described by σ/ν^s, where σ is related to the dc conductivity of the sample and s ($0 < s \leq 1$) is a fitting parameter.[17] For comparison, for low frequencies ($\nu < 10^{-2}$ Hz) relaxation data for PnBMA were added which were taken from ref 19.

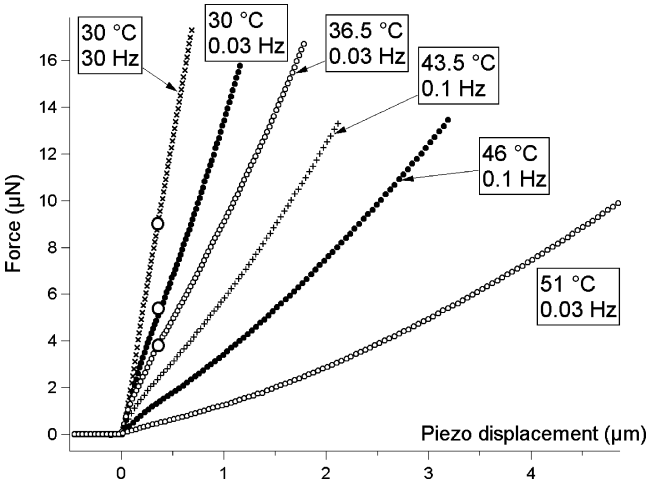

Figure 1. Approach force−displacement curves on the PnBMA at different temperatures and frequencies. As indicated also in the figure, the temperature and frequencies are (from left to right) 30 °C at 30 and 0.03 Hz, 36.5 °C at 0.03 Hz, 43.5 °C at 0.1 Hz, 46 °C at 0.1 Hz, and 51 °C at 0.03 Hz. In the first three curves the position of the yielding point, i.e., the point at which the stiffness (slope of the approach curve) decreases, is marked with a circle. In the other three curves the yielding point is near the origin and is not marked because it would lead to confusion. The yielding force decreases with increasing temperature and/or decreasing probe frequency. Also, the stiffness, both before and after the yielding point, decreases with increasing temperature and/or decreasing probe frequency.

The dielectric spectra show two relaxation processes indicated by peaks in the dielectric loss. The process at higher frequencies (lower temperatures) is the β-relaxation which corresponds to localized fluctuations of the carbonyl group, whereas the relaxation region at lower frequencies is the α-process related to the glass transition. The shift factor a_T is calculated by $a_T = \nu_m(T_{ref})/\nu_m(T)$ with $T_{ref} = 40$ °C.

Results and Discussion

Figure 1 shows six approach force−displacement curves acquired at different temperatures and frequencies (from left to right: 30 °C at 30 and 0.03 Hz, 36.5 °C at 0.03 Hz, 43.5 °C at 0.1 Hz, 46 °C at 0.1 Hz, and 51 °C at 0.03 Hz).

The dependence of the force on the distance during the approach (loading) phase will be analyzed in the following in detail, but some features can be pointed out immediately.

All acquired curves present a yielding point,[14] i.e., a critical force $F_{yield} = k_c\delta_{yield}$, at which the polymer starts undergoing a plastic deformation and the stiffness of the sample suddenly decreases. Such a force is observed as a kink in the approach contact line. For $F < F_{yield}$ the sample undergoes only elastic deformations, and only in this region elastic continuum contact theories can be applied.

Along the contact line the sample deformation D is given by

$$D = Z - \delta_c \tag{1}$$

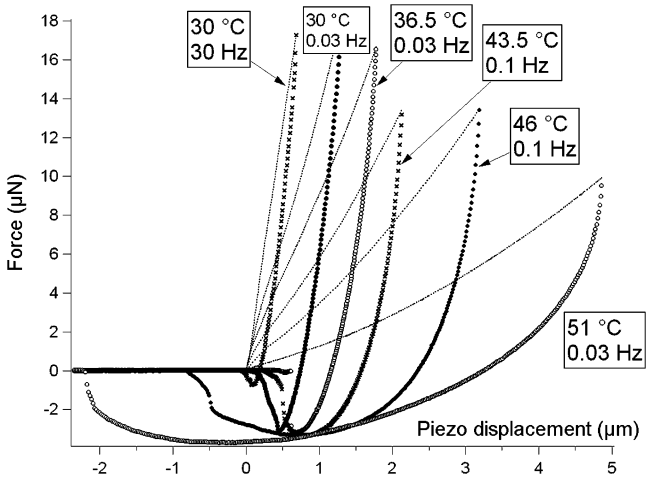

Figure 2. Retraction force−displacement curves (different markers) corresponding to the approach force−displacement curves in Figure 1 (continuous lines). The dissipated energy (area between approach and retraction curves above the zero axis), the permanent plastic deformation (intersection between the retraction curve and the zero axis), and the adhesion (area between the zero axis and the retraction curve) increase with increasing temperature and/or decreasing probe frequency.

where Z is the piezo displacement and δ_c is the cantilever deflection. If D is small, we can write[5]

$$k_c\delta_c = \frac{k_c k_s}{k_c + k_s} Z = k_{eff} Z \qquad (2)$$

where k_s is the sample elastic constant.

This simple approximation is valid only for small sample deformations, and this is not the case for most of the curves in this experiment, as can be seen in Figure 1. (The curves at high temperatures in Figure 1 show no linear dependence of F on Z.) An exact relation, based on elastic continuum theories, will be given in the following. Nevertheless, this simple relation shows that the slope of the approach force−displacement curve is an indicator for the stiffness of the sample. If the sample is much stiffer than the cantilever, i.e., $k_s \gg k_c$, $k_{eff} \cong k_c$, whereas $k_{eff} \cong k_s$ when $k_s \ll k_c$; i.e., the sample is much more compliant than the cantilever.

Observing the curves in Figure 1, two effects of temperature and frequency are immediately evident: the yielding force decreases with increasing temperature and/or probe time, and the stiffness of the sample, both before and after the yielding point, decreases with increasing temperature and/or probe time.

It is important to point out that the yielding force and the stiffness do not depend on the maximum force: all the curves at a certain temperature and frequency overlap with each other, independently of the maximum force.

Before we apply one elastic continuum contact theory, namely the Hertz theory,[7] to the approach force−displacement curves, we want to consider qualitatively the retraction force−displacement curves. Figure 2 shows the six retraction force−displacement curves corresponding to the approach curves shown in Figure 1.

Also for these curves, some features can be pointed out immediately. First of all, we can observe that the retraction contact line (unloading curve) does not overlap with the approach contact line. This happens because the sample has undergone a plastic deformation during the loading phase, as confirmed by the presence of a yielding point. During the unloading phase, the sample cannot regain its shape and the force exerted by the cantilever at every indentation depth is smaller than during the approach.[20−22] We can define three important quantities:[5,10,14] (1) The permanent plastic deformation δ_p is the intercept between the withdrawal contact line and the axis $F = 0$. The elastic recovery δ_e is the quantity $\delta_{max} - \delta_p$. For a totally elastic sample it would be $\delta_p = 0$ and $\delta_e = \delta_{max}$; for a totally plastic sample it would be $\delta_p = \delta_{max}$ and $\delta_e = 0$. (2) The elastic energy $\mathscr{E}$ is the area between the approach contact line and the axis $F = 0$. The dissipated energy $\mathscr{D}$ is the area between the two contact lines above the axis $F = 0$. $\mathscr{D} = 0$ and $\mathscr{D} = \mathscr{E}$ for a totally elastic and a totally plastic sample, respectively. (3) The work of adhesion W is the area between the axis $F = 0$ and the retraction force−displacement curve.

The curves in Figure 2 show that permanent plastic deformation, the dissipated energy, and the work of adhesion increase with temperature and/or probe time. This means that, by increasing the temperature and/or the probe time, the sample undergoes larger plastic deformations occurring at smaller forces, and consequently the dissipated energy and the work of adhesion, proportional to the tip−sample contact area, increase.

It is important to remember that, unlike the yielding force and the stiffness, δ_p, $\mathscr{D}$ and W depend also on the maximum force $F_{max} = k_c\delta_{max}$ exerted during the loading phase.

In the following, we will determine quantitatively the effect of temperature and frequency on the yielding force and on the stiffness. To this aim, we need to model both elastic and plastic deformations and to get from force−displacement curves quantities related to physical parameters describing the polymer sample.

To begin, we use the Hertz theory to model the elastic part of the loading curve. In the Hertz theory[7] the applied load and the deformation of the sample are related by the equation

$$F = k_c\delta_c = E_{tot}\sqrt{R}D^{3/2} = \frac{4}{3(1-\nu_P^2)}E\sqrt{R}D^{3/2} \Rightarrow$$
$$D^{3/2} = \frac{3(1-\nu_P^2)}{4}\frac{1}{E}\frac{k_c}{\sqrt{R}}\delta_c \qquad (3)$$

where R is the radius of the AFM tip, ν_P is the Poisson's ratio, and E is the Young's modulus of the sample, defined by

$$\frac{1}{E_{tot}} = \frac{3}{4}\left(\frac{1-\nu_P^2}{E} + \frac{1-\nu_t^2}{E_t}\right) \Rightarrow E_{tot} = \frac{4}{3(1-\nu_P^2)}E \qquad (4)$$

where ν_t and E_t are the Poisson's ratio and the Young's modulus of the tip. It is assumed that E_t is much larger than E.

In eq 3 has been assumed that the indenting tip has a spherical shape. Correction factors can be used to take into account the nonspherical shape, e.g., a paraboloidal shape, of the tip.[23]

All other elastic continuum contact theories predict the proportionality between $D^{3/2}$ and the force exerted by the cantilever, provided the forces are shifted by a factor depending on the adhesive force between tip and sample.[6] The differences in the resulting Young's modulus become very small when the adhesive force is

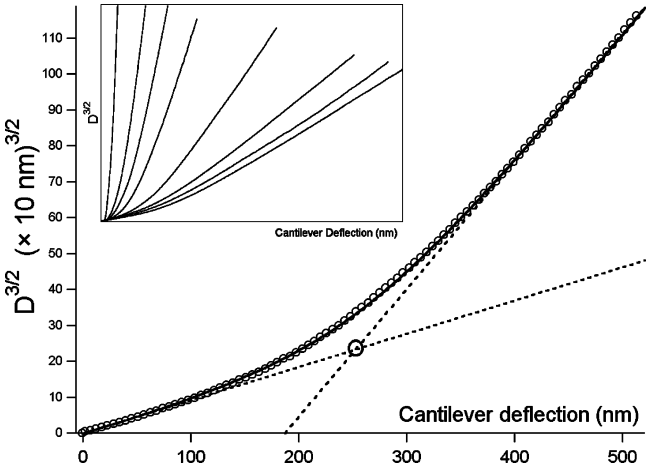

Figure 3. Fit of an average $D^{3/2}$ function at 30 °C and 30 Hz vs the cantilever deflection (open circles) with an hyperbola (eq 3) (thick continuous line). The figure shows also the linear regime limits for $\delta_c \ll \delta_{yield}$ and $\delta_c \gg \delta_{yield}$ and the intersection δ_{yield}. In the inset, the average functions $D^{3/2}$ at various temperatures and frequencies; from right to left: 30 °C at 30 Hz, 33 °C at 30 Hz, 36.5 °C at 30 Hz, 43.5 °C at 10 Hz, 43.5 °C at 1 Hz, 46 ° C at 1 Hz, and 51 °C at 1 and 0.03 Hz. With increasing temperature and/or probe time the slopes of both linear regimes increase (i.e., the stiffness decreases) and δ_{yield} decreases.

smaller than the applied load, and in this case, when modeling the loading curve, the effect of adhesion can be neglected.[24] Observing the curves in Figure 2, one could object that for high temperatures the adhesive force is comparable with the load, but this is due to the plastic deformation of the sample and to the increase of the contact area; i.e., this happens when the Hertz model cannot be applied. When Hertz model can be applied, i.e., in case of elastic deformations, the adhesive force is always smaller than the applied loads. The validity of this approach is confirmed by the agreement between AFM and DMA results, showing that the error introduced by neglecting the adhesive force is smaller than other ones, e.g., the error due to the heterogeneity of the sample or to the approximations in the values of the tip radius (see below).

Figure 3 shows the average $D^{3/2}$ calculated from a set of 100 curves at 30 °C and 30 Hz vs the cantilever deflection δ_c. The inset shows seven average functions $D^{3/2}$ vs the cantilever deflection at different temperatures and frequencies (from right to left: 30 °C at 30 Hz, 33 °C at 30 Hz, 36.5 °C at 30 Hz, 43.5 °C at 10 Hz, 43.5 °C at 1 Hz, 46 ° C at 1 Hz, and 51 °C at 1 and 0.03 Hz).

Instead of being proportional to δ_c, $D^{3/2}$ presents two linear regions. The first region is the elastic regime of the deformation. The slope of the second region is always larger than that of the first one. As shown in eq 3, the proportionality factor between $D^{3/2}$ and δ_c, i.e., the slope of the first (elastic) linear region, is inversely proportional to the Young's modulus of the sample. Hence, the increase in the slope corresponds to a decrease in the stiffness of the sample, as it should happen at $\delta_c = \delta_{yield}$. The two linear regions are connected by a third region where the slope gradually increases. The nonlinear region corresponds to the yielding point. If the polymer in the contact region were completely uniform, i.e., if chains of the same length had exactly the same bonds and entanglements with other chains, and also the stress in the contact area were uniform, the yielding point would be exactly a point and $D^{3/2}$ would be just the composition of two lines $y_1 = m_1\delta_c$ and $y_2 = m_2\delta_c + q$, with $m_2 > m_1$, intersecting at $\delta_c = \delta_{yield}$.

But the polymer and most of all the stress are not uniform,[9] so that there is a rather dispersed distribution of yielding points.

All these considerations lead to the idea of fitting $D^{3/2}$ functions where a yielding point, i.e., a plastic deformation, is present with an hyperbola function in the form

$$y = D^{3/2}(\delta_c) = (\beta\delta_c - \epsilon) + \sqrt{\alpha^2\delta_c^2 - 2\epsilon(\beta - \gamma)\delta_c + \epsilon^2} \tag{5}$$

with $\alpha > 0$, $\beta > 0$, $\gamma > 0$, $\epsilon > 0$, and $\beta - \alpha < \gamma < \beta + \alpha$. This last condition comes from the requirement that $D^{3/2}$ has real values for $\delta_c > 0$, i.e., $\alpha^2\delta_c^2 - 2\epsilon(\beta - \gamma)\delta_c + \epsilon^2 > 0$ for $\delta_c > 0$.

In the two regions where $D^{3/2}$ and δ_c are proportional, i.e., for $\delta_c \ll \delta_{yield}$ and $\delta_c \gg \delta_{yield}$, we can approximate the hyperbola with two lines, i.e., its tangent at $\delta_c = 0$ and its asymptote for $\delta_c \to \infty$, respectively:

$$\delta_c \ll \delta_{yield} \Rightarrow y \cong y'(0)\delta_c \Rightarrow D^{3/2} \cong \gamma\delta_c$$

$$\delta_c \gg \delta_{yield} \Rightarrow y \cong (\lim_{\delta_c\to\infty} y')\delta_c +$$

$$\lim_{\delta_c\to\infty} (y - \delta_c y') \Rightarrow D^{3/2} \cong (\beta + \alpha)\left[\delta_c - \frac{\epsilon}{\alpha}\left(1 - \frac{\gamma}{\alpha + \beta}\right)\right] \tag{6}$$

and δ_{yield} can be defined as the intersection of the two lines, given by

$$\delta_{yield} = \epsilon/\alpha \tag{7}$$

It is important to point out the physical meaning of such a fit. This model is an interpretation of a yielding region, and hence of a plastic deformation, as a gradual transition from a first elastic deformation $D^{3/2} \cong \gamma\delta_c$ to a second deformation with lower stiffness in the form $D^{3/2} - \gamma\delta_{yield} = (\alpha + \beta)(\delta_c - \delta_{yield})$. The plastic deformation, showing the same dependence on the load as an elastic deformation with proportionality coefficient $\alpha + \beta$, is added to the elastic deformation obtained at F_{yield} ($\gamma\delta_{yield}$) and is caused by the force $k_c(\delta_c - \delta_{yield})$. Hence, by changing the origin of the $D^{3/2}$ vs δ_c plot, a plastically deformed polymer can be treated, from the mathematical point of view, as an elastically deformed polymer with smaller stiffness.

All average $D^{3/2}$ vs δ_c plots acquired at different temperatures and frequencies have been fitted with this model. As a result, we obtained the coefficients $\alpha + \beta$, γ, and δ_{yield} as functions of the temperature T and of the frequency ν; i.e., for each of the seven temperatures, we obtain a curve (isotherm) of the coefficients, e.g., $\alpha + \beta$, vs the frequency. Figure 4 shows the seven isotherms obtained for the quantity $[3(1 - \nu_P^2)/4][1/(\alpha + \beta)] = 0.67/(\alpha + \beta)$ as a function of $\log(\nu)$. The factor 0.67 has been calculated by assuming for the Poisson's ratio of the polymer a usual value of 0.33.

Most of the isotherms have more than one point at a certain temperature and frequency. These are the results of the fit of curves acquired at the same temperature and frequency, but on different locations on the sample, and prove that the sample is rather homogeneous and that the measured elastic−plastic quantities do not depend on the topography.

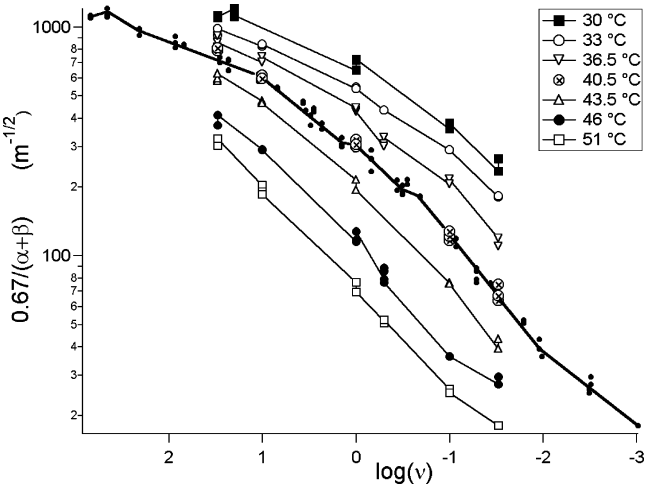

Figure 4. Isotherms of the quantity $0.67/(\alpha + \beta)$, proportional to the stiffness after the yielding point, as a function of $\log(\nu)$ (the versus of the X-axis is inverted). From top to bottom: 30, 33, 36.5, 40.5, 43.5, 46, and 51 °C. Lines are only a guide for the eye. The points on the thick continuous line are the same isotherms shifted of the quantities $\log(a_T)$ until they overlap and so yielding the master curve. The thick continuous line is only a guide for the eye.

The measured isotherms can be used to obtain a master curve for the given quantity. The procedure is based on the time−temperature superposition principle: the effect of a shift of temperature is equivalent to a certain shift of the probe time for most of the physical properties of a polymer. Practically, chosen a certain reference temperature T_{ref} or reference isotherm (in our case 40.5 °C), every isotherm is shifted of a quantity $\log(a_T)$ until it overlaps with the reference isotherm. A shift to the left corresponds in our case to an increase of the frequency (a decrease of the probe time) and hence a decrease of the temperature. The overlapping isotherms yield the master curve, i.e., the given quantity as a function of frequency or, equivalently, of temperature. Figure 4 shows also the obtained master curve for the quantity $0.67/(\alpha + \beta)$.

The temperature dependence of the shift values $\log(a_T)$ satisfies the Williams−Landel−Ferry equation:[25]

$$\log a_T = \frac{-C_1(T - T_{ref})}{C_2 + (T - T_{ref})} \tag{8}$$

where C_1 and C_2 are two constants.

The data obtained by means of AFM measurements are in very good agreement with the data obtained by means of dynamic mechanical analysis and broadband spectroscopy, also shown in Figure 5.

The parameters calculated from the DMA data are $C_1 = 17.3$ and $C_2 = 154$ °C. If $T_{ref} \cong T_g$, then usually $C_1 \cong 11$ and $C_2 = 50$ °C. The discrepancy in the constant C_1 depends on the fact that the reference temperature has not been chosen near the glass temperature. The unusual value of the parameter C_2 is a peculiarity of poly(n-alkyl methacrylate)s. The glass transition temperature of this class of polymers decreases strongly with increasing length of the side group. Moreover, also a strong broadening of the thermal glass transition range with increasing length of the side group is observed.[26] From the dielectric point of view the class of poly(n-alkyl methacrylate)s behave quite unusually compared to other amorphous polymers. This is due to

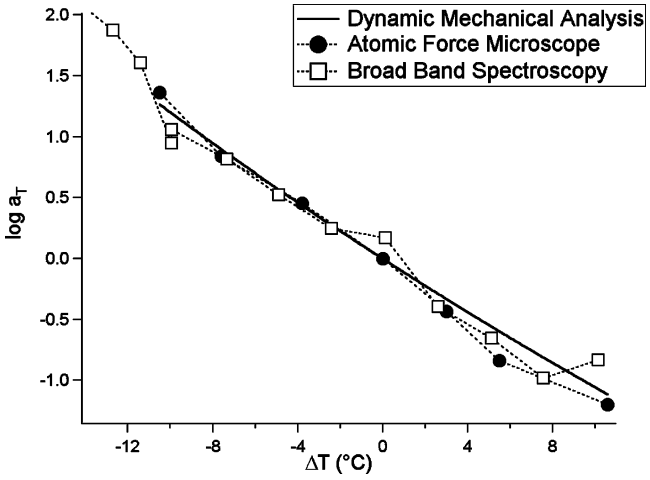

Figure 5. Shift values $\log(a_T)$ vs $\Delta T = T - T_{ref}$. The AFM data (full circles) are shown together with DMA (continuous line) and broadband spectroscopy (squares) data.

the dielectric strength of the β-process, which is found to be higher than that of the α-relaxation. The reason for this behavior is unclear up to now. Since the main dipole moment is located in the side group, just small fluctuations of it can contribute significantly to the dielectric loss. But there is some evidence from NMR-measurements that this might be due to coupled motion of the main and of the side chain.[28] It might be that the unusual values of the Williams−Landel−Ferry parameters are related to the peculiarities of the relaxation behavior of the poly(n-alkyl methacrylate)s.[28]

All the parameters measured with AFM force−displacement curves, in particular γ and δ_{yield}, obey the Williams−Landel−Ferry equation with the same coefficients C_1 and C_2.

From the parameter γ it is possible to calculate the Young's modulus of the sample following the Hertz theory. As already shown, for $\delta_c \ll \delta_{yield}$ it is

$$D^{3/2} \cong \gamma\delta_c \Rightarrow E \cong \frac{3(1 - \nu_P{}^2)}{4} \frac{k_c}{\sqrt{R}} \frac{1}{\gamma} \tag{9}$$

For $\delta_c \gg \delta_{yield}$, we can write

$$D^{3/2} = (a + \beta)\left[\delta_c - \left(1 - \frac{\gamma}{\alpha + \beta}\right)\delta_{yield}\right] \Rightarrow$$
$$D^{3/2} - \gamma\delta_{yield} = (a + \beta)(\delta_c - \delta_{yield}) = (a + \beta)\bar{\delta}_c \Rightarrow$$
$$\bar{E} = \frac{3(1 - \nu_P{}^2)}{4} \frac{k_c}{\sqrt{R}} \frac{1}{(\alpha + \beta)} \tag{10}$$

As already pointed out, $\bar{E}$ is the proportionality factor between the additional deformation $D^{3/2} - \gamma\delta_{yield}$ and the "reduced" force $F = k_c(\delta_c - \delta_{yield}) = k_c\bar{\delta}_c$ during the plastic deformation, i.e., after the yielding point. This parameter can be seen as an analogue of the usual Young's modulus for the elastic deformation, but only from the mathematical point of view.

Figure 6 shows the Young's modulus E and the parameter $\bar{E}$ calculated from AFM data together with the Young's modulus calculated from DMA data. The moduli are shown in a logarithmic scale vs the logarithm of the frequency and vs the temperature (the two quantities are equivalent thanks to the Williams−Landel−Ferry equation).

For the calculation it is necessary to know the value of the elastic constant of the cantilever k_c and of the tip

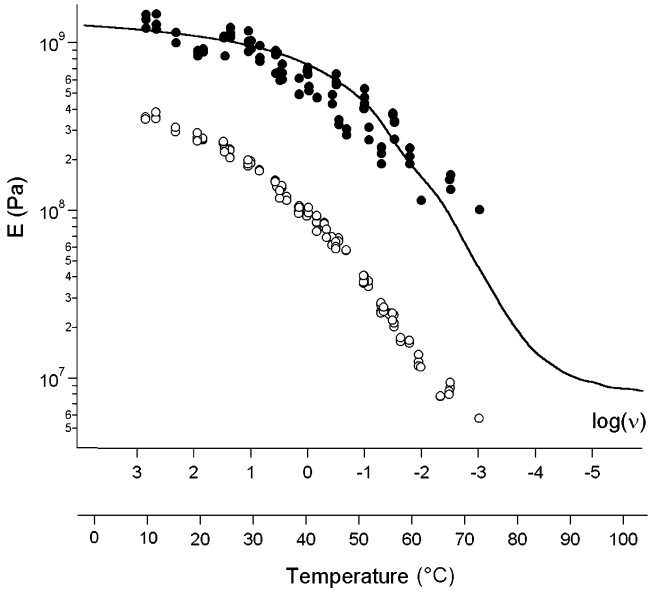

Figure 6. Young's modulus E (full circles) and its analogue after the yielding point $\bar{E}$ (open circles) calculated from AFM data together with the Young's modulus calculated from DMA data (continuous line). The moduli are shown in a logarithmic scale vs the logarithm of the frequency and vs the temperature, calculated through the William−Landels−Ferry equation.

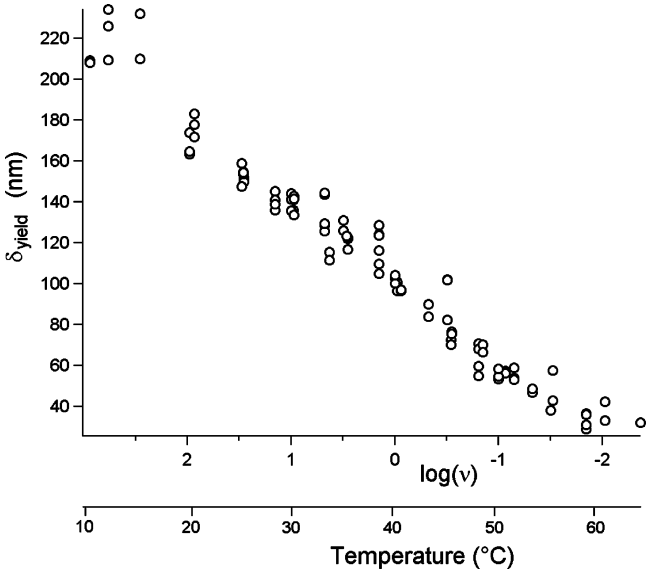

Figure 7. Master curve of δ_{yield} vs the frequency and vs the temperature.

radius R. The elastic constant has been measured from the noise spectrum of the cantilever[5] and is $k_c = 45$ N/m. The tip radius has not been measured. Rather, it has been chosen so that the AFM data match the DMA data. Figure 5 shows the moduli obtained with $R = 20$ nm. For $R = 20 \pm 5$ nm there is a rather good agreement. The value given by the manufacturers is $R = 10$ nm.

Even if the Hertz model with a spherical tip is for our tip−sample system a rather rough approximation, the two measurements are in a rather good agreement. Some errors due to the approximation are eventually compensated by the choice of R. To our knowledge, this is the first measurement of the dependence of the Young's modulus of a polymer on temperature performed with an AFM. The comparison with the results obtained through a customary method like DMA is particularly important and allows the conclusion that not only T_g but also the curve $E(\nu)$ or $E(T)$, i.e., the Young's modulus as a function of temperature and/or frequency, can be determined by means of AFM force−displacement curves.

For the glass temperature T_g, defined as the maximum of E''/E', where E' (E'') is the storage (loss) modulus, the DMA measurements give the value of 22 °C, in agreement with the value given by the suppliers. It is important to point out that the stiffness of the sample does not depend linearly on the temperature and that the change of the stiffness is not abrupt and does not define a single point, i.e., a single temperature or frequency, rather a transition region where the stiffness gradually changes from the value of the glassy state to that of the rubbery state. Hence, the characterization of the whole curve $E(\nu)$ or $E(T)$ gives much more information than the determination of the glass temperature as a point at which the elastic−plastic properties of the polymer abruptly change[4] and provides a much more realistic picture of the dependence of the elastic−plastic properties on temperature, without simplifying and reducing it to a discrete transition.

As already pointed out, all the parameters determined through the fit of $D^{3/2}$ obey the Williams−Landel−Ferry equation with the same coefficients C_1 and C_2. It is interesting to characterize the dependence of the yielding point δ_{yield}. The master curve of δ_{yield} vs the frequency and vs the temperature is shown in Figure 7.

For very low temperatures and very high frequencies $\delta_{yield} > 200$ nm, and hence $F_{yield} > 9$ μN. The yielding indentation δ_{yield} decreases linearly with increasing temperature, and for high temperatures and/or low frequencies $\delta_{yield} < 40$ nm, i.e., $F_{yield} < 1.8$ μN.

It is important to understand whether the distribution of the yielding points can be so large that it influences the stiffness also for $\delta_c \cong 0$. It is a straightforward task to verify that $\{\partial(D^{3/2})\}/\partial\delta_c$ is a sigmoid with plateau values $\beta - \alpha$ and $\beta + \alpha$. Hence, if $(\beta + \alpha - \gamma)/2\alpha \cong 1$ or $(\beta - \gamma)/\alpha \cong 1$, the value of the stiffness at $\delta_c \cong 0$ can be considered independent from the stiffness after the yielding point. On the other hand, if $(\beta - \gamma)/\alpha \cong 0$, some polymer chains yield also for very low forces; i.e., their stiffness goes over to the lower value already at small loads, and the stiffness is always influenced by yielding and plastic deformations. The factor $\alpha/(\beta - \gamma)$ can be considered as the width of the first derivative $\{\partial(D^{3/2})\}/\partial\delta_c$. Our experimental data show that $(\beta - \gamma)/\alpha$ is nearly 1 only at low temperatures and/or high frequencies (until about 1 Hz at 40.5 °C) and then starts decreasing down to 0.4 at 51 °C and 0.03 Hz.

These considerations lead to three important conclusions: (1) Increasing the temperature and/or the probe time, more and more polymer chains yield also for very low forces and the difference between the usual Young's modulus E and the parameter $\bar{E}$ corresponding to the additional plastic deformation becomes smaller and smaller, as can be observed also in Figure 6. (2) If only small indentations are performed, it is impossible to determine the stiffness after the yielding point and its influence on the stiffness before the yielding point; hence, the determination of the stiffness before the yielding point and of the Young's modulus is affected by large errors. (3) At high temperatures and/or probe times δ_{yield} decreases and the width of the first derivative increases. As a consequence, the value of the

stiffness is influenced by the yielding also at very low forces because a large portion of the polymer chains yields also for very low loads. Hence, the stiffness before yielding and the Young's modulus can be calculated only if the value of the stiffness after the yielding point is known, and performing large indentations is particularly necessary.

Some considerations can be done also for the elastic energy, i.e., the energy stored in the sample during the loading phase. Remembering that the elastic energy $\mathcal{E}$ is the area between the approach curve and the X-axis, that $D = Z - \delta_c$, and that for $\delta_{max} \ll \delta_{yield}$ $D = \gamma^{2/3}\delta_c^{2/3}$, we can write

$$\frac{\mathcal{E}}{k_c} = \int_0^{D_{max}} \delta_c \, dZ = Z_{max}\,\delta_{max} - \int_0^{\delta_{max}} Z \, d\delta_c = \gamma^{2/3}{\delta_{max}}^{5/3} + {\delta_{max}}^2 - \int_0^{\delta_{max}} (\gamma^{2/3}{\delta_c}^{2/3} + \delta_c) \Rightarrow \frac{\mathcal{E}}{k_c} - \frac{1}{2}{\delta_{max}}^2 = \frac{2}{5}\gamma^{2/3}{\delta_{max}}^{5/3} \quad (11)$$

The expression for $\delta_{max} \gg \delta_{yield}$, where $D = (\alpha + \beta)^{2/3}[\delta_c - (1 - \gamma/(\alpha + \beta))\delta_{yield}]^{2/3}$, is

$$\frac{\mathcal{E}}{k_c} - \frac{1}{2}{\delta_{max}}^2 = \frac{2}{5}(\alpha+\beta)^{2/3}\left[\delta_{max} - \left(1 - \frac{\gamma}{\alpha+\beta}\right)\delta_{yield}\right]^{2/3} \times \left(\delta_{max} + \frac{3}{2}\left(1 - \frac{\gamma}{\alpha+\beta}\right)\delta_{yield}\right) - \frac{3}{5}\gamma^{2/3}\left(1 - \frac{\gamma}{\alpha+\beta}\right){\delta_{yield}}^{5/3} \quad (12)$$

Note that, since the piezo displacement Z and the sample deformation D are related by eq 1, the only difference between the area under a force vs piezo displacement curve ($Z_{max}\delta_{max} - \int Z \, d\delta_c$) and the area under a force vs sample deformation curve ($D_{max}\delta_{max} - \int D \, d\delta_c$) is the factor ${\delta_{max}}^2 - \int \delta_c \, d\delta_c = {}^1/_2{\delta_{max}}^2$. Hence, the quantity $\mathcal{E} - {}^1/_2 k_c{\delta_{max}}^2$ is the elastic energy taken from force vs sample deformation curves.

Figure 8 shows the measured values of $\mathcal{E}/k_c - {}^1/_2{\delta_{max}}^2$ at 30 °C and 30 Hz as a function of δ_{max} and the functions in eqs 11 and 12 calculated with the parameters $\alpha + \beta$ and γ obtained from the fit of $D^{3/2}$. The calculated values of the energy are in very good agreement with the experimental data for $\delta_{max} \ll \delta_{yield}$ or $\delta_{max} \gg \delta_{yield}$. The elastic energy cannot be integrated only in the transition or yielding region. As a matter of fact, the elastic energy could be used to determine the fit parameters $\alpha + \beta$ and γ, and the stiffness could be calculated from the plot of E vs δ_{max}, but the fit is not so precise like in the case of $D^{3/2}$.

The inset of Figure 8 shows plots of the elastic energy vs δ_{max} at different temperatures and frequencies (30 Hz at 33 °C, 0.1 Hz at 33 °C, and 0.03 Hz at 36.5, 40.5, 43.5, 46, and 51 °C). The elastic energy at a given δ_{max} is proportional to the parameters $\gamma^{2/3}$ or $(\alpha + \beta)^{2/3}$, and it increases with temperature and/or decreasing frequency.

Conclusions

The most important result of the present work is the quantitative characterization of the dependence of the Young's modulus of PnBMA on temperature or, equivalently, on frequency by means of AFM force−displacement curves. The characterization of the function $E(T)$ gives much more information than the determination of the glass temperature.

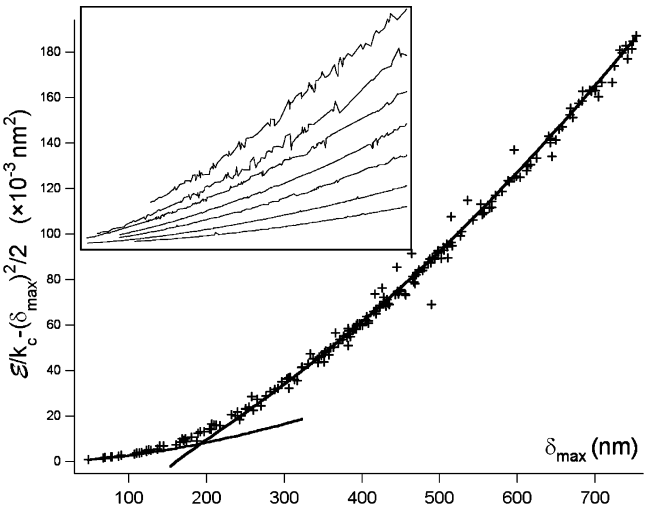

Figure 8. Experimental values of $\mathcal{E}/k_c - {}^1/_2{\delta_{max}}^2$ at 30 °C and 30 Hz vs δ_{max} (markers) and the functions in eqs 11 and 12 calculated with the parameters $\alpha + \beta$ and γ obtained from the fit of $D^{3/2}$ (thick continuous lines). In the inset, the quantities $\mathcal{E}/k_c - {}^1/_2{\delta_{max}}^2$ vs δ_{max} at various temperatures and frequencies; from bottom to top: 30 Hz at 33 °C, 0.1 Hz at 33 °C, and 0.03 Hz at 36.5, 40.5, 43.5, 46, and 51 °C. With increasing temperature and/or probe time the elastic energy increases.

It has been shown that AFM force−displacement curves can be a powerful tool also for the determination of local values of other viscoelastic quantities, such as the yielding force as a function of the temperature and/or of the frequency.

All measured quantities have been compared with the results of customary, well-established techniques, e.g., broadband spectroscopy and dynamic mechanical analysis in the case of the Williams−Landel−Ferry coefficients and dynamic mechanical analysis in the case of the Young's modulus. In both cases there is a very good agreement.

For the analysis of the deformations of the polymer samples the proportionality between $D^{3/2}$ and δ_c, predicted by all elastic continuum contact theories and giving information on the stiffness and on the Young's modulus of the sample, has been extended successfully to plastic deformations. In this way, the yielding of the polymer is considered as a gradual transition to deformations with lower stiffness, resulting from the distribution of different yielding forces for different sample portions inside the tip−sample contact area. Such a model can be used to fit both elastic and plastic deformations of the sample and other related quantities, e.g., the elastic energy. All the parameters and quantities determined with help of this model, i.e., the Young's modulus before the yielding, the analogue of the Young's modulus after the yielding, corresponding to plastic deformations, and the yielding force, obey to the Williams−Landel−Ferry equation with the same coefficients.

Some important technical details about the technique have been also found. In particular, it has been shown that at very high temperatures and/or very low frequencies the yielding force reaches very small values and the transition region becomes very large, so that plastic deformations occur also for very small loads and also the stiffness at very small loads is influenced by the

stiffness after the yielding point, i.e., the stiffness corresponding to plastic deformations. In other words, at very high temperatures and/or very low frequencies it is not possible to avoid plastic deformations of the sample, and it is advantageous to perform large indentations with large plastic deformations, so that their influence on the stiffness at small loads can be determined.

Acknowledgment. The authors thank Dr. W. Stark (Federal Institute for Material Testing and Research) for the DMA measurements and Dr. A. Schönhals (Federal Institute for Material Testing and Research) for the broadband spectroscopy measurements.

References and Notes

(1) Dinelli, F.; Buenviaje, C.; Overney, R. M. *Thin Solid Films* **2001**, *396*, 138.
(2) Marti, O.; Stifter, T.; Waschipky, H.; Quintus, M.; Hild, S. *Colloids Surf. A* **1999**, *154*, 65.
(3) Tsui, O. K. C.; Wang, X. P.; Ho, J. Y. L.; Ng, T. K.; Xiao, X. *Macromolecules* **2000**, *33*, 4198.
(4) Bliznyuk, V. N.; Assender, H. E.; Briggs, G. A. D. *Macromolecules* **2002**, *35*, 6613.
(5) Cappella, B.; Dietler, G. *Surf. Sci. Rep.* **1999**, *34*, 1.
(6) Maugis, D. *J. Colloid Interface Sci.* **1992**, *150*, 243.
(7) Hertz, H. *J. Reine Angew. Math.* **1881**, *92,* 156.
(8) Derjaguin, B. V.; Müller, V. M.; Toporov, Yu. P. *J. Colloid Interface Sci.* **1975**, *53*, 314.
(9) Johnson, K. L.; Kendall, K.; Roberts, A. D. *Proc. R. Soc. London A* **1971**, *324*, 301.
(10) Briscoe, B. J.; Fiori, L.; Pelillo, E. *J. Phys. D* **1998**, *31*, 2395.
(11) Chizhik, S. A.; Huang, Z.; Gorbunov, V. V.; Myshkin, N. K.; Tsukruk, V. V. *Langmuir* **1998**, *14*, 2606.
(12) Reynaud, C.; Sommer, F.; Quet, C.; El Bounia, M.; Duc, T. M. *Surf. Interface Anal.* **2000**, *30*, 185.
(13) Raghavan, D.; Gu, X.; Nguyen, T.; VanLandingham, M. R.; Karim, A. *Macromolecules* **2000**, *33*, 2573.
(14) Du, B.; Tsui, O. K. C.; Zhang, Q.; He, T. *Langmuir* **2001**, *17*, 3286.
(15) Domke, J.; Radmacher, M. *Langmuir* **1998**, *14*, 3320.
(16) VanLandingham, M. R. *Microsc. Today* **1997**, *97*, 12.
(17) Kremer, F.; Schönhals, A. *Broadband Dielectric Spectroscopy*; Springer-Verlag: Berlin, 2002.
(18) Havriliak, S.; Negami, S. *J. Polym. Sci., Part C* **1966**, *14*, 99.
(19) Garwe, F.; Schönhals, A.; Lockwenz, H.; Beiner, M.; Schröter, K.; Donth, E. *Macromolecules* **1996**, *29*, 247.
(20) Cappella, B.; Sturm, H.; Schulz, E. *J. Adhes. Sci. Technol.* **2002**, *16*, 921.
(21) Cappella, B.; Sturm, H. *J. Appl. Phys.* **2002**, *91*, 506.
(22) Munz, M.; Cappella, B.; Sturm, H.; Geuss, M.; Schulz, E. *Adv. Polym. Sci.* **2003**, *164*, 87.
(23) Akhremitchev, B. B.; Walker, G. C. *Langmuir* **1999**, *15*, 5630.
(24) Johnson, K. L.; Greenwood, J. A. *J. Colloid Interface Sci.* **1997**, *192*, 326.
(25) Williams, M. L.; Landel, R. F.; Ferry, J. D. *J. Am. Chem. Soc.* **1955**, *77*, 3701.
(26) Hempel, E.; Beiner, M.; Renner, T.; Donth, E. *Acta Polym.* **1996**, *47*, 525.
(27) Kulik, A. S.; Beckham, H. W.; Schmidt-Rohr, K.; Radloff, D.; Pawelzik, U.; Boeffel, C.; Spiess, H. W. *Macromolecules* **1994**, *27*, 4746.
(28) Beiner, M. *Macromol. Chem. Rapid Commun.* **2001**, *22*, 869.

MA040135F